STEADY-STATE REGULATION OF SECRETORY CARGO EXPORT BY INOSITOL TRISPHOSPHATE RECEPTORS AND PENTA EF HAND PROTEINS

Aaron Held[1], John Sargeant[1], Jennet Hojanazarova[1], Corina Madreiter-Sokolowski[2], Roland Malli[2], Wolfgang F. Graier[2], and Jesse C. Hay[1]

[1]Division of Biological Sciences, Center for Structural & Functional Neuroscience, University of Montana, USA; [2]Molecular Biology and Biochemistry, Gottfried Schatz Research Center, Medical University of Graz, Austria

correspondence: jesse.hay@umontana.edu

ABSTRACT

Ca^{2+} release by inositol trisphosphate receptors (IP3Rs) regulates diverse physiological processes in many cell types. Notably, agonist-stimulated Ca^{2+} signaling involving IP3Rs can modulate ER export rates through activation of the Ca^{2+}-dependent adaptor ALG-2. It is unknown, however, whether IP3Rs and ALG-2 regulate ER export rates at steady state. Here we report that partial depletion of IP3Rs from normal rat kidney (NRK) epithelial cells caused a marked increase of ER export of the transmembrane cargo VSV-G. Depletion of IP3R-3, the major IP3R isoform in NRK cells, had a larger impact on secretion than the other extant isoform, IP3R-1. Under standard growth conditions, spontaneous cytosolic Ca^{2+} oscillations usually occurred simultaneously in successive groups of contiguous cells, generating intercellular Ca^{2+} waves (ICWs) that moved across the monolayer. Unexpectedly, IP3R-3-depleted cells exhibited increased cell participation in this spontaneous signaling. IP3R-3-depleted cells also exhibited increased agonist-dependent Ca^{2+} signaling, suggesting a general potentiation of the remaining IP3R channels. Increased spontaneous signaling was accompanied by increased ALG-2 and decreased peflin at ER exit sites (ERES), resulting in increased targeting of COPII coat to ERES. Furthermore, the increased secretion rate associated with IP3R depletion required ALG-2. Unexpectedly, IP3R depletion also resulted in partial depletion of ER luminal Ca^{2+} stores, though this phenomenon was not involved in the secretion change. We conclude that in NRK cells, IP3Rs regulate spontaneous Ca^{2+} signaling that helps determine the basal secretion rate by modulating COPII targeting to ERES. Furthermore, the IP3R channel density and/or isoform

composition significantly impacts this phenomenon.

INTRODUCTION

Calcium is a vital intracellular signaling molecule integral for a diverse array of physiological processes. Regulatory roles for Ca^{2+} in intracellular trafficking steps are still being elucidated. Recent work on ER-to-Golgi transport demonstrates involvement of luminal Ca^{2+} stores at a stage following cargo biogenesis and folding/assembly, apparently through the release of Ca^{2+} into the cytoplasm where it binds and activates the vesicle budding, docking and/or fusion machinery (1, 2). Effector mechanisms by which cytosolic Ca^{2+} modulates ER-to-Golgi transport appear to involve penta-EF-hand-containing (PEF) protein adaptors that have been implicated in many Ca^{2+}-dependent cellular phenomena (3). The PEF protein apoptosis-linked gene-2 (ALG-2) acts as a Ca^{2+} sensor at ER exit sites (ERES) and can stabilize the association of the COPII coat subunit Sec31A with the membrane when Ca^{2+} is present (4-7). However, regulation of ER cargo export by ALG-2 and Ca^{2+} does not follow the simple pattern suggested by these early studies. For one thing, sustained agonist-driven Ca^{2+} signaling results in a sharp ALG-2-dependent reduction of COPII targeting and ER export (8). For another, ALG-2 in cell extracts often exists in a stable heterodimer with another PEF protein - peflin - that binds ALG-2 in a Ca^{2+}-inhibited manner (9, 10). The peflin-complexed form of ALG-2 appears to bind ERES, destabilize the COPII coat and suppress ER export, but through a distinct mechanism than during sustained Ca^{2+} signals (8, 11). Release of ALG-2 from either of these inhibitory states appears to switch its activity, causing it to stimulate COPII targeting and ER export; this switch can be induced by short-lived - as opposed to continuous - Ca^{2+} signals (8). To summarize, it appears that Ca^{2+} signals, depending upon strength and duration, can induce either stimulatory or inhibitory actions of ALG-2 at ERES.

But what governs ALG-2 actions at steady state? ER Ca^{2+} signals at steady state may be due to spontaneous Ca^{2+} oscillations mediated by gated Ca^{2+} channels, e.g. (12) - which have been shown to dynamically alter ALG-2 localization (6) - or else by continuous ER leak, for example mediated by presenilin-1 (13, 14) and/or the translocon (15, 16). Furthermore, a recent study in goblet cells, another polarized epithelial cell type, found that spontaneous cytosolic Ca^{2+} oscillations requiring ryanodine receptor (RyR) Ca^{2+} channels provide a steady-state signal acting as a tonic brake to mucin granule exocytosis (17). In this case, however, the Ca^{2+} sensor

was apparently KChIP3 localized to pre-exocytic secretory granules. Clearly much remains to be learned about steady-state ER Ca^{2+} signals and their effectors throughout the secretory pathway.

Since IP3 receptors, during agonist-driven Ca^{2+} signaling, contribute to PEF protein-mediated regulation of ER export, we wondered whether spontaneous Ca^{2+} signals due to IP3Rs at steady state might also contribute to setting the basal ER export rate. Here we demonstrate that depletion of IP3R-3, the major IP3R isoform in normal rat kidney (NRK) epithelial cells, increases the basal ER export rate of the COPII cargo VSV-G_{ts045} by up to 70% while at the same time causing more prevalent spontaneous cytoplasmic Ca^{2+} oscillations. The stimulatory effect on transport is blocked in the absence of ALG-2 and is accompanied by a decrease of peflin and increase of ALG-2 and COPII coat at ERES. In conclusion, this work indicates that spontaneous Ca^{2+} oscillations favor the stimulatory ALG-2 activity at ERES and help establish the basal secretion rate. Furthermore, the abundance of IP3Rs or the mix of isoforms influences secretion by determining the propensity for these Ca^{2+} oscillations.

RESULTS

Depletion of IP3Rs accelerates ER-to-Golgi transport

To characterize the expression of IP3R isoforms in NRK cells, immunoblotting was performed using antibodies to all three individual IP3R isoforms - IP3R-1, IP3R-2, and IP3R-3. Both IP3R-1 and IP3R-3 were readily detectable in NRK extracts, but IP3R-2 was undetectable (data not shown). To determine the ratio of IP3R-1 and IP3R-3 in NRK cells, qRT-PCR was carried out on NRK cell total RNA using isoform-specific primers. As shown in Figure 1A, IP3R-3 was the major isoform, representing 67% of all IP3R subunits; the ratio of IP3R-3:IP3R-1 was thus 2:1 in NRK cells. Using isoform-specific siRNAs, either IP3R-3 or IP3R-1 could be depleted by ~95% (Figure 1B). IP3Rs form both functional homo-tetramers and functional hetero-tetramers (12, 18). Hence, IP3R-3 depletion would largely eliminate IP3R-3 homo-tetramers and IP3R-3-containing hetero-tetramers, leaving only IP3R-1 homo-tetramers, representing about a third of the normal number of channels. Likewise, IP3R-1 depletion would leave only IP3R-3 homo-tetramers representing about two-thirds of the normal number of total channels. Knockdown of both isoforms simultaneously was technically feasible, however, this

caused cytopathic effects including slow growth and an abnormal ER architecture with swollen ER tubules (not shown). Since it would be difficult to interpret transport changes in the context of this highly abnormal ER, we did not further characterize the complete absence of IP3R channels.

To test the effects of IP3R depletion on ER-to-Golgi cargo transport, we used an intact-cell transport assay (2, 8, 11, 19) employing the temperature-sensitive transmembrane cargo VSV-G_{ts045} to measure the average rate of transport during the first 12 minutes following shift to the transport-permissive temperature of 32 ºC. Figure 1C shows example images and illustrates the morphological principle of the assay. Importantly, as demonstrated quantitatively in Figure 1D, knockdown of the major IP3R isoform, IP3R-3, resulted in up to a ~70% acceleration of the ER-to-Golgi transport rate. Knockdown of the lesser isoform, IP3R-1, resulted in a less dramatic, though still highly significant, ~20% increase in transport. Taken together these results indicate that under steady-state conditions, both IP3R channel isoforms affect the rate of ER-to-Golgi transport, roughly in proportion to their abundance. Further characterization of effects of IP3R depletion were carried out only on the dominant IP3R-3 isoform.

IP3R depletion down-regulates PEF protein expression but does not alter expression of multiple other trafficking machineries

To investigate the mechanism of the increased secretion, we asked whether IP3R depletion caused increased transport by virtue of increased expression of trafficking machinery proteins. In particular, one could imagine that altered ER Ca^{2+} handling could result in unfolded protein response (UPR) activation which is known to increase expression of COPII-related components. We first examined relevant gene expression using qRT-PCR. As shown in Figure 2A, IP3R-3 knockdown did not significantly affect mRNA expression of COPII inner coat components Sec24A, B, C, or D, nor outer shell component Sec31A, nor ERES scaffolds Sec16A and B. There was perhaps a trend toward an increase of Sec24C, but it was not statistically significant and not supported by immunoblotting of cell extracts (see below). Overall, the qRT-PCR data did not support general up-regulation of ERES components as would be expected if basal UPR signaling were higher. In addition, we found that none of the UPR-related genes ATF6, CHOP, or Grp78 were affected by IP3R depletion. We found that ALG-2 and peflin were expressed at very similar levels and not affected by IP3R depletion at the transcript level. Finally, Bcl-2

transcripts were reduced by a highly significant ~30% upon IP3R-3 depletion; this demonstrates that IP3R-3 depletion had an effect on a gene product known to directly interact with and regulate the activity of IP3Rs (20). We complimented this analysis with immunoblotting of NRK cells extracts transfected with control or IP3R-3 siRNAs. As seen in Figure 2B, UPR mediators phospho-EIF2α, phospho-IRE-1 and ATF4 did not noticeably change upon IP3R depletion. Turning to the transport machinery, Figure 2C demonstrates no changes in coat subunits Sec31A, ß-COP, Sec24c, Sec23, the ER/Golgi tether p115, cargo receptors ERGIC-58 (labeled "p58") and p24. These results indicate that IP3R depletion did not increase transport by increasing the expression of the required transport machinery. However, we also observed in immunoblots a small yet consistent decrease in both ALG-2 and peflin. This effect was quantified from multiple biological and technical replicates and displayed in Figure 2D, revealing on average a ~25% decrease in both proteins. Since mRNA levels were not affected (Figure 2A), it appears that this change occurs via a post-transcriptional mechanism. Note that concomitant reduction of both total cellular ALG-2 and peflin is not predicted to in and of itself significantly change transport, since the two are still present in the same ratio. However, since both proteins are unstable when not in the ALG-2-peflin heterodimer (10) which is disrupted by elevated Ca^{2+} (9), this finding could indicate that there is a higher Ca^{2+}environment in the IP3R knockdown condition creating greater flux between the ALG-2 heterodimer and homodimer forms.

IP3R depletion causes increased ALG-2 and Sec31A, but decreased peflin targeting to ERES

The potentially increased flux of ALG-2 complexes during IP3R-3 depletion (Figure 2D) led us to ask whether ALG-2 and peflin targeting to ERES was altered, since this could change COPII coat targeting and thus ER export. ALG-2 binds Sec31A at ERES either as a peflin-containing hetero-oligomer, most like the known heterodimer, or as a peflin-lacking species, most likely the known homodimer. While the peflin-lacking species can be either stimulatory or inhibitory, the ALG-2-peflin hetero-oligomer is inhibitory (8). We carried out immunofluorescence of endogenous ALG-2, peflin, and Sec31A on control and IP3R-3-depleted NRK cells. For a non-COPII-related marker of ERES we used rBet1, an ER/Golgi SNARE whose distribution is mostly restricted to ERES and ERGIC elements (21). Representative images of cells are shown in Figure 3A-C. We segmented the labeling patterns into discrete

objects by thresholding and then used Boolean image math to measure the areas of objects and areas of co-localization between objects representing different proteins in the same cell (8, 11). As shown in Figure 3D, when IP3R-3 was depleted, co-localization between peflin and rBet1 objects decreased by ~25%. The decreased co-localization was comprised of both a decrease in the percentage of total peflin objects that co-localized with rBet1, and a decrease in the percentage of total rBet1 objects that co-localized with peflin (data not shown); this reciprocity of effects, which was also true in parts E and F, establishes a true decrease in co-localization that could not result from mere changes in labeling intensity or expression. At the same time, co-localization between ALG-2 and rBet1 significantly increased by ~35% in IP3R-3-depleted cells (Figure 3E). Focusing on the outer coat, we found that the co-localization area of Sec31A and rBet1 increased by ~50% upon IP3R-3 depletion (Figure 3F). The expansion of Sec31A-rBet1 overlap most likely indicates that more outer coat was recruited to ERES, consistent with past work concluding that ALG-2 'stabilized' the outer coat at ERES (4, 7). Taken together all immunofluorescence changes during IP3R depletion - decreased peflin, increased ALG-2 and increased Sec31A recruitment to ERES - predict and mechanistically account for the elevated levels of ER-to-Golgi transport.

Effects of IP3Rs on ER-to-Golgi Transport are mediated by ALG-2

To further examine the role of ALG-2 in the IP3R depletion-dependent increase in secretion, we combined depletion of IP3Rs with that of ALG-2. As demonstrated in the ER-to-Golgi transport assay Figure 4B, IP3R-3 depletion in otherwise wildtype cells increased transport by ~60% (bars 1 vs. 2), consistent with Figure 1D. However, in ALG-2-depleted cells, depletion of IP3R-3 caused no further significant effect (bars 3 vs. 4, p=.257). This is the result expected if ALG-2 is required to mediate the increased transport due to IP3R depletion; ALG-2 is epistatic to IP3Rs for transport effects.

An alternative way to view the data is relative to the effects of ALG-2 depletion. ALG-2 can either stimulate or inhibit transport, depending upon peflin expression levels and Ca^{2+} signaling patterns (8). In otherwise wildtype cells, depletion of ALG-2 increased transport (bars 1 vs. 3), indicating that ALG-2 complexes were acting as a net inhibitor of transport in wildtype cells. On the other hand, in IP3R-3-depleted cells, depletion of ALG-2 decreased transport (bars 2 vs. 4), indicating that ALG-2 was acting as a stimulator of transport in IP3R-3-depleted cells. Hence,

depletion of IP3R-3 switched the roles of ALG-2 complexes from that of a net inhibitor to that of a net stimulator of transport. Since peflin expression levels did not change relative to ALG-2 (Figure 2D), the likely explanation for this switch is altered Ca^{2+} patterns in IP3R-3-depleted cells.

IP3R depletion caused increased spontaneous Ca^{2+} oscillations

Previous work on Ca^{2+} signals and secretion in NRK cells indicated that a strong pulse of cytosolic Ca^{2+} caused by the sarco-endoplasmic reticulum Ca^{2+} ATPase (SERCA) inhibitor 2,5-Di-(*t*-butyl)-1,4-hydroquinone (BHQ) followed by near-baseline Ca^{2+} for $\geq$ 2 hours led to an ALG-2-dependent increase in transport similar to that observed in Figures 1D and 4B for depletion of IP3Rs (8). We wondered whether changes in the IP3R channel density and/or isoform mix might have altered basal signaling to produce Ca^{2+} patterns similar in principle to those caused by BHQ that stimulated ER export. However, it was not possible to predict from the literature whether IP3R-3 depletion would increase or decrease basal signaling; some literature suggests that decreased overall IP3R channel density should decrease basal signaling (22), while other literature suggests that specific depletion of the IP3R-3 isoform, per se, should increase basal signaling (12, 23, 24). To answer this question ourselves we monitored cytoplasmic Ca^{2+} in NRK cells using the Ca^{2+}-sensitive dye FURA-2AM; cells were recorded for 20 min at 37 ^{o}C in regular growth medium containing 10% FBS in the absence of added agonists. As illustrated by representative individual cell traces in Figure 5A, some cells displayed a short burst of Ca^{2+} oscillations during the 20-minute interval. We created individual traces for all 514 cells in the image field, and determined that 52 cells or 10.1% displayed at least one burst of signaling; each burst contained 1-6 distinct oscillations in which each oscillation persisted for about 1 minute. Though it was not technically feasible to monitor for longer periods, we assume that over longer time intervals the majority of NRK cells would display similar episodes of spontaneous Ca^{2+} signaling.

Intercellular coordination of Ca^{2+} signaling was typically observed in these recordings, which were performed on confluent NRK monolayers very similar to those used in our secretion studies. Coordination took the form of groups of contiguous or nearby cells that oscillated almost precisely in unison. Furthermore, in many cases successive groups of activated cells would spread laterally over time, creating waves of high Ca^{2+} that traversed the monolayer.

Figure 5B shows a group of 338 cells containing the same cells plotted in Figure 5A, with their individual locations marked. Figure 5C displays the same group of cells at several distinct timepoints during the recording with the $R_{340/380}$ ratio displayed using a heatmap for contrast. In detail, cell 26 initiated a major Ca^{2+} wave at t = 04:44, when cells 118 and 126 joined and oscillated in unison a few seconds behind cell 26. Five to ten cells at a time then oscillated together in successive groups that led upward and to the right across the field, culminating in cells 238, 241, 282 and others oscillating in unison at t = 7:44 before the wave moved further rightward and out of view. The continuous nature and high local participation in this intercellular Ca^{2+} wave (ICW) is better appreciated in the video (Supplementary Video File 1) containing all 150 timepoints during the first 10 minutes of the recording. The mechanism and functions of ICWs are not well understood; they can be driven by both cell-to-cell diffusion of Ca^{2+} and IP3 through gap junctions and also by paracrine purinergic signaling (PPS) involving vesicular and non-vesicular release of the Ca^{2+} agonist ATP (25). While we did not investigate the mechanisms of NRK cell ICWs further, we speculate that one relevant consequence of ICWs is that they may amplify cell participation in spontaneous, steady-state Ca^{2+} signaling.

We compared control and IP3R-3-depleted NRK cells for their participation in spontaneous, steady-state Ca^{2+} signaling using recordings similar to that described above. Each of the 300-500 cells in the view area of each run was analyzed using a semi-automated workflow in ImageJ and R that generated individual Ca^{2+} traces that could be scrolled through rapidly for manual scoring; each trace was scored for the number of spontaneous Ca^{2+} oscillations, from which the percentage of cells participating in oscillations was derived for each run. As shown in Figure 5D, which represents scoring of ~23,000 cells in 49 individual runs, IP3R-3-depleted cells exhibited significantly higher cell participation in spontaneous signaling, increasing about three-fold, from 5.5% to 16% cell participation during a 20-minute period. Though it was not possible to objectively score ICWs *per se*, a majority of recordings displayed groups of cells oscillating synchronously, indicating that intercellular coordination or spread of Ca^{2+} oscillations may be a major driver of participation in basal Ca^{2+} signaling in NRK cells. The specific recording shown in Figure 5A-C is highlighted in the composite plot (5D) with a cyan halo. While this recording displayed the linear cell-to-cell spread of signaling unusually clearly, it was not remarkably active in terms of cell participation, which ranged much higher among IP3R-3-depleted cells. We also compared the number of oscillations per cell among participating cells between control

and IP3R-3-depleted cells, and found that there was a trend toward greater numbers of oscillations in IP3R-3-depleted cells (Figure 5E). In conclusion, IP3R depletion caused increased spontaneous Ca^{2+} oscillations, facilitated through intercellular spread, that potentially drove the ERES composition changes noted in Figure 3 and resulted in the increased secretion documented in Figure 1D and 4B.

IP3R depletion caused potentiation of agonist-dependent Ca^{2+} signaling

The increased spontaneous activity of IP3Rs following partial depletion led us to ask whether they might also be more excitable in response to Ca^{2+} agonists. As demonstrated in Figure 6A, which displays representative FURA cell traces, most NRK cells responded to 1 uM bradykinin with a single synchronous surge of Ca^{2+} followed by a fall-off in Ca^{2+} during the ensuing 2-3 minutes. About 20% of cells did not visibly respond (back trace), and cells with multiple, distinct oscillations were infrequently seen (not shown). Figure 6B-D displays results of systematic comparisons of control and IP3R-3-depleted cells using the bradykinin protocol from part A. Notably, as shown in Figure 6B, a significantly greater percentage of IP3R-depleted cells responded to bradykinin, raising the participation rate from ~80 % to ~95 %. Additionally, as shown in Figure 6C, IP3R-3-depleted cells responded with significantly higher amplitude Ca^{2+} surges than control cells, represented by a ~40 % increase in amplitude. We also integrated the entire Ca^{2+} response, from onset of signaling until returning to baseline, among responding cells only, which demonstrated a highly significant ~20 % increase in Ca^{2+} release (Figure 6D). This result eliminates the possibility that the change in amplitude was driven solely by a different shape of the Ca^{2+} response over time. In summary, both spontaneous and evoked Ca^{2+} responses were potentiated in the partially IP3R-3-depleted cells. Our results are reminiscent of a study of NRK fibroblasts (a distinct cell line from our epithelial NRK cells) where depletion of IP3R-3 caused increased frequency of Ca^{2+} oscillations as well as Ca^{2+} action potentials in response to prostaglandin $F_2\alpha$ (24).

IP3R depletion caused decreased ER luminal Ca^{2+} stores, a phenomenon unrelated to the increase in ER export

We also characterized ER luminal Ca^{2+} stores in control and IP3R-depleted cells using D1ER, a genetically encoded ER luminal FRET-based Ca^{2+} sensor (26). The initial, basal FRET ratio,

R_0, varied arbitrarily between individual NRK cells - perhaps due to different expression levels and/or sensor aggregation, precluding the ability to directly measure resting Ca^{2+} levels. Therefore all data points, R, were normalized relative to their initial value, R_0. As shown by representative traces in Figure 7A, upon addition of ionomycin and EGTA to live NRK cells, R/R_0, which for the first five minutes has a value near 1, quickly plunged and approached an R_{min}/R_0 value; R_{min}/R_0 ranged from ~0.75 (for control cells) to ~0.85 (for IP3R-depleted cells). The difference between the initial R/R_0 and R_{min}/R_0, - or $\Delta R/R_0$ - was interpreted to represent the resting ER luminal Ca^{2+} concentration of the cell. As shown in Figure 7B, which combines cells from multiple replicate experiments, $\Delta R/R_0$ was ~28 % lower in IP3R-depleted cells. To verify the conclusion using a different approach, we used an irreversible sarco-endoplasmic reticulum Ca^{2+} ATPase (SERCA) inhibitor, 1 μM thapsigargin (Tg), to release all ER Ca^{2+}, and then measured the magnitude of the resulting cytoplasmic Ca^{2+} surge in NRK cells transfected with the genetically encoded FRET-based cytosolic Ca^{2+} sensor D3cpv (27). As shown in Figure 7C and D, IP3R-3-depleted NRK cells displayed smaller Ca^{2+} releases, by approximately 33 %, upon Tg addition, consistent with the conclusion that ER Ca^{2+} stores were partially depleted. We also used a similar Tg addition protocol together with a genetically encoded FRET-based mitochondrial matrix Ca^{2+} sensor, 4mtD3cpv (28), and found that mitochondria took up less Ca^{2+} upon release of ER Ca^{2+} in IP3R-depleted cells (data not shown). Together these experiments indicate that, for reasons that are not obvious, depletion of IP3Rs in NRK cells results in partial depletion of ER Ca^{2+} stores. We do not believe the increased spontaneous signaling was responsible; although further speculations on the molecular cause of the Ca^{2+} depletion are offered in the Discussion, we did not pursue its mechanism further.

A reasonable interpretation is that the increased spontaneous cytosolic Ca^{2+} transients documented in Figure 5 drive the ERES changes displayed in Figure 3 which cause the increased secretion established in Figure 1. The reduced luminal Ca^{2+} presents a challenge to the interpretation, since it cannot be eliminated that the reduced luminal store *per se* somehow regulates the transport machinery by an unknown mechanism, perhaps involving luminal Ca^{2+}-binding proteins. If this were the case, comparably reduced luminal Ca^{2+} stores would still stimulate transport, even without depletion of IP3Rs and increased cytosolic Ca^{2+} oscillations. We experimentally created such a condition by treating cells with very low levels of Tg, two orders of magnitude below the concentrations typically used to induce UPR. As shown in Figure

8A and B, 6 nM Tg for 24 hours resulted in partial depletion of luminal Ca^{2+} similar to that caused by IP3R-3 siRNA, while at 10 nM, the Tg caused greater depletion. We used 24 hours to simulate any potential long-term effects on secretion as well as to get well beyond any stimulatory effects caused by the initial wave of released ER Ca^{2+}. We then tested the effects of these partial ER Ca^{2+} depletions on ER-to-Golgi transport. As shown in Figure 8C, there were no significant effects on transport at 6 nM Tg, but ~20% inhibition of transport became apparent at 10 nM Tg. Inhibition of ER-to-Golgi transport under conditions of strong ER depletion is expected from previous results, wherein up to 40% inhibition of transport was observed after ER Ca^{2+} was reduced by 85%, from the resting value of ~386 μM, to ~56 μM (1, 2). The lack of transport effects at 6 nM demonstrates that partial luminal Ca^{2+} depletion for ~24 hours *per se* does not drive the increased transport observed in IP3R-depleted cells. In conclusion, the data favor the interpretation that increased spontaneous cytosolic Ca^{2+} oscillations, and not the lowered Ca^{2+} store, primarily drives the PEF protein changes that result in increased transport when IP3Rs are depleted.

DISCUSSION

IP3Rs and steady-state Ca^{2+} signals regulate protein secretion from the ER

Here we demonstrated that unexpectedly, IP3R-dependent Ca^{2+} signals are a rate-limiting factor setting the basal secretion rate in resting epithelial cells under normal growth conditions. This adds significantly to the previously reported role of IP3Rs in secretion, in which agonist-dependent activation of IP3Rs can either increase or decrease the secretion rate depending upon the intensity and duration of signaling (8). The new data demonstrates that periodic, spontaneous Ca^{2+} signals, facilitated in part by intercellular Ca^{2+} waves (ICWs), provide a stimulus that determines how much ALG-2 and peflin are bound at ERES, which alters COPII targeting and thus ER export.

One consequence of this work is that physiological factors known to affect spontaneous signaling or ICWs, such as Bcl-2 family protein expression (29), presenilin-1 mutation (30), or gap junctions, hemichannel function, and purinergic receptor expression (25), may also regulate the secretion rate through this mechanism. Furthermore, we demonstrated that this phenomenon is sensitive to expression levels and/or the mix of isoforms of IP3Rs present, with lower expression levels of IP3Rs, particularly of the IP3R-3 isoform, favoring more spontaneous

signaling and higher secretion rates. Factors that affect IP3R expression and turnover include micro-RNAs (31, 32), phosphatase and tensin homolog (PTEN) (33), BRCA1 associated protein (BAP1) (34), nuclear factor erythroid 2–related factor 2 (NRF2) (35), and NF-κB (36). These factors could potentially regulate the secretory export rate through the mechanism presented here.

Additionally, physiological phenomena known to be driven by spontaneous Ca^{2+} signaling could have changes in ER export as part of their mechanism. These phenomena could include glial control of neurovascular diameter (37, 38), nephron formation during kidney development (39), and numerous aspects of neural proliferation, migration, and differentiation during neocortical development (37, 40). While these phenomena involve spontaneous signaling, in most cases it is not known whether ICWs *per se* play a functional role. Retinal epithelial pigment cells are one cell type where ICWs have been established to regulate cell fate, influencing retinal development (25). Regulation of secretory output could be a significant effector mechanism by which ICWs alter cell fates in retinal or other cell types with ICWs. The biosynthetic secretory pathway is a rate-limiting determinant of plasma membrane and organelle biogenesis, plasma membrane composition, secretion of signaling molecules, and cell growth. Additionally, diseases associated with changes in IP3R expression, for example spinocerebellar ataxia (31), atherosclerosis (41), various liver disorders (42), and multiple cancer types including uveal melanoma, mesothelioma (43), colorectal carcinoma (44), and breast cancer (45, 46), could also have a secretory component to their pathophysiology. However, it should be noted that we have not tested whether other cell types besides NRK cells exhibit the strong link between spontaneous Ca^{2+} signaling and the secretion rate. This is an area for further investigation.

Also note that "spontaneous" and "steady-state" are operational terms. We refer to spontaneous Ca^{2+} signaling as that which occurs in unperturbed cells growing in DMEM containing 10% FBS. The ultimate source of the signals could well be trace agonists, for example serotonin present in typical lots of FBS that has been shown to elevate phospholipase C activity in a distinct (from ours) line of NRK cells (47). We did not conduct Ca^{2+} signaling experiments in the complete absence of potential extracellular agonists since that condition would not provide the factors that our ER-to-Golgi transport studies require.

Mechanism of effects on ER-to-Golgi transport

This work elucidates a role for basal IP3R-propagated Ca^{2+} signals in setting the rate of ER export by modulating the activities and/or targeting of the PEF proteins ALG-2 and peflin at ERES. Ca^{2+} binding to PEF proteins may directly modulate their propensity to bind each other and/or Sec31A. For example, if increased Ca^{2+} signals cause formation of ALG-2 homodimers at the expense of the ALG-2/peflin heterodimer (9) and/or favor homodimer binding to Sec31A over heterodimer, then no further explanation would be needed to explain our observations. Indeed, this explanation fits the prevailing concept that high Ca^{2+} favors binding of the ALG-2 homodimer - the presumptive stimulatory species in secretion - to its effectors (48). However, we also uncovered that decreases in peflin and ALG-2 protein abundance occur when IP3Rs are depleted. This suggests that Ca^{2+} may in addition alter the species at ERES through altered stability or turnover of distinct PEF protein complexes. For example, if higher Ca^{2+} destabilizes heterodimeric ALG-2 and peflin, this could lead to a higher relative abundance of ALG-2 homodimers and thus an acceleration of secretion. This hypothesis is supported by previous *in vitro* observations that heterodimer formation stabilizes both proteins against rapid proteasomal degradation (10), but that high Ca^{2+} causes dissociation of the heterodimer (9). It is also consistent with the relatively slow onset of secretion changes following agonist-induced Ca^{2+} signaling, first detectable after 30 minutes and increasing over several hours (8). Ca^{2+}-dependent changes in ALG-2 and peflin binding to ERES and Ca^{2+}-dependent destabilization of heterodimers are mutually compatible mechanisms that may both contribute to regulation of the steady-state secretion rate.

Roles of ER luminal Ca^{2+} in vesicle transport

Luminal ER Ca^{2+} appears to impact ER-to-Golgi transport on several levels. We have known for 30 years that a substantial ER Ca^{2+} store is required for proper folding and quality control of many, but not all protein cargos (49). More recently, Ca^{2+} chelator and SERCA inhibitor studies have indicated that luminal Ca^{2+} is also required for ER-to-Golgi vesicle transport *per se* independently of cargo biosynthesis and folding (1, 2, 50). Under severe luminal Ca^{2+} depletion conditions, COPII buds and unfused vesicles accumulate at ERES, and transport is inhibited by ~ 40% (2). It is not known whether ALG-2 and peflin are involved in this apparent requirement for nominal luminal Ca^{2+}, or alternatively whether more fundamental aspects of secretion, such as maintenance of proper membrane fluidity or fusogenic lipids require this minimal level of

luminal Ca^{2+}. On the other hand, ALG-2 and peflin are completely dispensable for secretion (8), but appear to adapt the secretory rate to Ca^{2+} signals released into the cytoplasm. In conclusion, ER Ca^{2+} appears to have several roles in biosynthetic secretion, one subset of which are mediated through ALG-2 and peflin when Ca^{2+} is released into the cytosol.

The fact that IP3R depletion caused a mild reduction of luminal Ca^{2+} is challenging to interpret, since store-operated Ca^{2+} entry (SOCE) should be more than fast enough to compensate for the periodic Ca^{2+} oscillations we observed in resting NRK cells. One interpretation would be that IP3Rs play a specific role in SOCE in NRK cells. Indeed, a direct role of IP3Rs in SOCE in *Drosophila* has been demonstrated (51); however, their direct role in SOCE in mammalian cells, though widely discussed, is not well-supported (22). Furthermore, IP3R inhibitors such as 2-Aminoethoxydiphenyl borate (2-APB) and xestospongins cannot be conveniently used to clarify the role of IP3Rs in SOCE, or aid in the present studies, since they also inhibit SOCE and SERCA, apparently independently of IP3Rs (18). Though we did not pursue the mechanism of the effects on Ca^{2+} stores, control experiments in Figure 8 allowed us to determine that the mild changes in luminal Ca^{2+} caused by IP3R siRNAs did not appear to drive the effects we observed on ER-to-Golgi transport.

EXPERIMENTAL PROCEDURES

Antibodies

Mouse monoclonal anti-mannosidase II antibody was purchased from Covance Research Products (Denver, PA; product MMS-110R-200). Rabbit polyclonal anti-IP3R-1 antibody was purchased from ThermoFisher Scientific (Waltham, MA; product PA1-901). Mouse monoclonal anti-IP3R-3 antibody was purchased from BD Biosciences (San Jose, Ca^{2+}; item 610313). Anti-rbet1 mouse monoclonal antibody, clone 16G6, was as described (21). Rabbit polyclonal anti-peflin and chicken polyclonal anti-ALG-2 were produced previously (8). Rabbit polyclonal anti-sec31A, anti-sec23, anti-p24 and anti-β-Cop were produced previously against synthetic peptides (1, 52). Rabbit polyclonal anti-Phospho-eIF2α antibody was purchased from Cell Signaling Technology (Danvers, MA; product 9721s). Rabbit polyclonal anti Phospho-IRE1 was purchased from Abcam (Cambridge, United Kingdom; item ab48187. Rabbit polyclonal anti-ATF4 antibody was purchased from GeneTex (Irvine, Ca^{2+}; product GTX101943). Rabbit polyclonal anti-sec24c was a kind gift from Dr. William Balch (Scripps Institute). Rabbit

polyclonal anti-p115 was produced in-house (53). Rabbit polyclonal anti-p58 was a kind gift from Dr. Jaakko Saraste (University of Bergen, Norway). Secondary antibody congugates with Alexa Flour™ 488 were from Invitrogen (Carlsbad, CA; product A11001). Cy3- and cy5-conjugated secondary antibodies were purchased from Jackson ImmunoResearch Laboratories (West Grove, PA).

qRT-PCR

NRK cells were transfected with IP3R-3 siRNA (see below) using Transfast (Promega Corp.; Madison WI) using manufacturer's instructions. Total RNA was isolated using the PEQLAB total RNA isolation kit (Peqlab; Erlangen, Germany) and reverse transcription was performed in a thermal cycler (Peqlab) using a cDNA synthesis kit (Applied Biosystems; Foster City, CA). mRNA levels were examined by qRT-PCR. A QuantiFast SYBR Green RT-PCR kit (Qiagen; Hilden, Germany) was used to perform real time PCR on a LightCycler 480 (Roche Diagnostics; Vienna, Austria), and data were analyzed by the REST Software (Qiagen). Relative expression of specific genes was normalized to human GAPDH as a housekeeping gene. Primers for real time PCR were obtained from Invitrogen (Vienna, Austria).

siRNA knockdowns and transfections

For transport experiments and Ca^{2+} measurements, NRK cells were electroporated with 0.6 µM siRNA and grown in DMEM with 4.5 g/L glucose containing 10% fetal calf serum and 1% penicillin-streptomycin. After 2-3 days of normal growth at 37 ºC, the cells were resuspended and re-electroporated, this time with a combination of the siRNA plus 7.5 µg of VSV-G-GFP plasmid. Cells were allowed to recover and grow on coverslips at 41 ºC for 24 h. For all non-transport experiments the same protocol was performed, but after specific plasmid transfection, cells were allowed to recover and grown on coverslips at 37 °C.

Alternatively, for the immunofluorescence experiments (Figure 3), sub-confluent cells grown on glass coverslips in 6-well plates were directly transfected without resuspension. After ~16 h incubation in OptiMEM containing 0.3% RNAiMax (Invitrogen; Carlsbad, CA) and 0.28 µM siRNA, transfection medium was supplemented with an equal part of OptiMEM containing 5% fetal calf serum, 2 mM $CaCl_2$, and 1% penicillin-streptomycin and incubated for another 3-5 hours. Subsequently, this post-transfection medium was removed (but saved) and replaced with

DMEM containing 10% fetal calf serum, 1% penicillin-streptomycin, 0.3% PolyJet (SignaGen Laboratories; Frederick, MD) , and 1 µg/ml plasmid. After ~12 h incubation, the plasmid solution was removed, cells were washed twice with PBS and returned to their siRNA-containing OptiMEM medium to recover while continuing the knockdown for another 24 h.

There was no noticeable difference in knockdown or transfection efficiency between the two transfection protocols. Cells from all transfections were either lysed directly in SDS-PAGE sample buffer for quantitative immunoblotting, or else processed for transport, colocalization, or FRET assays as described below.

Custom siRNAs were purchased from Ambion/Thermo Fisher (Waltham, MA) or Gene Link (Elmsford, NY) and contained no special modifications. We used two different siRNAs for IP3R-3 which appeared to perform similarly in knockdown efficiency and effects on Ca^{2+} and secretion; the large majority of experiments were performed using siRNA Itpr3-7848 (5' GCA GAC UAA GCA GGA CAA A dTdT 3'). siRNA Itpr3-0452 (5' GGA UGU GGA GAA CUA CAA A dTdT 3') was used intermittently for confirmation purposes. ALG-2 siRNA was described and its effects on secretion confirmed previously (2, 11). Control siRNAs were custom synthesized non-targeting siRNAs from the same manufacturer. Immunoblotting of cell lysates enabled validation of knockdown efficiencies for each siRNA experiment that was functionally analyzed.

ER-to-Golgi transport assay

NRK cells were transfected with plasmid and/or siRNA as described above and plated on poly-L-lysine coated coverslips. After 24 hours of cargo plasmid expression at 41 ºC, the cells were either fixed by dropping coverslips directly into fixative or into 6-well chambers containing pre-equilibrated 32 ºC medium for 12 min, then transferred to fixative. Coverslips were fixed and labeled using anti-mannosidase II antibody as described in the immunofluorescence section below. Morphological quantitation of ER-to-Golgi transport was accomplished as described previously (8, 11). Briefly, images were collected in a consistent manner with regard to cell morphology, protein expression levels and exposure. A single widefield image plane was collected for each color channel (GFP and mannosidase II) for each field of cells randomly encountered; image deconvolution was not performed. Images were analyzed using ImageJ open source image software with automation by a custom script (available upon request) that

randomizes the images and presents them to the user in a blind fashion. The user identifies transfected cells and subcellular regions while the script extracts parameters including extracellular background, Golgi intensity and diffuse cytoplasmic ER intensity. Transport index is calculated for each individual cell as ($Golgi_{max}$ - background) / (ER_{mean} - background), and all extracted parameters are written to an appendable output file along with a cell number and image title so that the data was traceable. Using this method, the user quantitates about 60 cells per hour. Once transport indices have been obtained for all conditions in an experiment, each value is subtracted by the mean transport index value for cells that were fixed directly from 41 ºC without a transport incubation at 32 ºC (typically a value between 1.0 and 1.5) to generate the net transport index. Net transport indices are then normalized to the mean siControl value for the particular experiment, prior to plotting and comparison between experiments. Each result reported here was obtained in at least three separate experiments on different days.

Immunofluorescence microscopy

Coverslips were fixed with 4% paraformaldehyde containing 0.1 M sodium phosphate (pH 7.0) for 30 min at room temperature and quenched twice for 10 min with PBS containing 0.1 M glycine. Fixed cells were treated for 15 min at room temperature with permeabilization solution containing 0.4% saponin, 1% BSA, and 2% normal goat serum dissolved in PBS. The cells were then incubated with primary antibodies diluted in permeabilization solution for 1 h at room temperature. Next, coverslips were washed 3x with permeabilization solution and incubated 30 min at room temperature with different combinations of Alexa Flour™ 488-, Cy3-, and/or Cy5-conjugated anti-mouse, anti-rabbit, or anti-chicken secondary antibodies. After the secondary antibody incubation, coverslips were again washed 3x using permeabilization solution and mounted on glass slides using Slow Fade Gold antifade reagent (Invitrogen product S36936) and the edges sealed with nail polish. Slides were analyzed using a 40x or 60x objective on a Nikon E800 widefield microscope with an LED illumination unit (CoolLED pE 300^{white}), sCMOS PCO.edge 4.2 camera, Prior excitation and emission filter wheels and Z-drive, automated using Micro-Manager software.

Colocalization Assays

For immunofluorescence co-localization experiments, fixed NRK cells such as in Figure 3

were captured using a 60x/1.40 Plan Apo objective as z-stacks in eleven 200-nm increments for each color channel. Image stacks were deconvolved using Huygens Essential Widefield software (Scientific Volume Imaging, Hilversum, The Netherlands). Final images for display and quantitation represent maximum intensity projections of deconvolved stacks. ERES area was assessed by a custom ImageJ script (available upon request). Briefly, background labeling was removed by defining a dark extracellular area of each channel image as zero. For each cell an object binary image mask (excluding the nucleus) was generated for each individual channel by auto thresholding using the 'Moments' (for rbet1) or 'Renyi Entropy' (for ALG-2, Peflin, and sec31) algorithms. Next, each channel mask was compared to the other using a Boolean 'and' operation to create a co-localization binary mask. The total object area for each mask was extracted and written to an appendable output file along with the cell number and image title so that the data was traceable. Colocalization areas for each cell were then normalized to the mean siControl value for the particular experiment, prior to plotting and comparison as reported in Figure 3.

Calcium Imaging

Subconfluent NRK cells growing on glass coverslips were transfected with genetically encoded Ca^{2+} sensors D1ER or D3cpv and siRNA as described above and imaged the next day. In some experiments (Figures 5 and 6) control or knockdown cells were loaded with FURA-2-AM for 30 minutes at 37°C directly prior to imaging, rather than transfection with a Ca^{2+} sensor. Coverslips were placed in a perfusion chamber and imaged on a Nikon TE300 inverted microscope equipped with a 40x objective, motorized high speed Sutter Lambda filter wheel for emissions, CoolLED pe340 excitation system, and PCO Panda sCMOS camera, automated with Micro-Manager software. Imaging was carried out using various perfusion protocols as described below with imaging at 3 or 4-second intervals. For examination of basal Ca^{2+} oscillations as in Figure 5, cells were labeled with FURA-2AM and imaged for 20 minutes in stagnant DMEM containing 10% FBS maintained at ~37°C. For examination of agonist-dependent Ca^{2+} signaling as in Figure 6, cells were labeled with FURA-2AM and imaged for a total of 10 minutes with a constant perfusion rate of 2 ml/min at room temperature. After 5 minutes of DMEM, the perfusion solution was changed to DMEM + 1 μM bradykinin. Each FURA imaging interval involved collecting an image at 510 nm emission and 340 or 380 nm

excitation. For all other protocols, each imaging interval involved collecting images at 480 nm and 530 nm using 430 nm excitation. For examination of ER luminal Ca^{2+} stores as in Figure 7A, cells were transfected with D1ER and imaged for a total of 12 minutes with a constant perfusion rate of 2 ml/min at room temperature. After 5 min of $2Ca^{2+}$ buffer (2 mM $CaCl_2$, 138 mM NaCl, 1mM $MgCl_2$ 5 mM KCl, 10 mM D-glucose, 10 mM Hepes, pH 7.4), the buffer was changed to $0Ca^{2+}$ buffer (138 mM NaCl, 1 mM $MgCl_2$, 5mM KCl, 10 mM D-glucose, 0.1 mM EGTA, 10 mM Hepes, pH 7.4) + 3 µM Ionomycin. For examination of cytosolic Ca^{2+} release as in Figure 7C, cells were transfected with D3cpv and imaged for a total of 15 minutes with a constant perfusion rate of 2 ml/min at room temperature. After 5 minutes, the $2Ca^{2+}$ buffer was changed to $2Ca^{2+}$ buffer + 200 nM Thapsigargin (Tg). For analysis in ImageJ, each cell, as well as an extracellular background region was enclosed in an ROI and mean intensity was collected in each color channel at each time interval. Data was imported to Kaleidagraph software, where the intensity data was converted to ratios. For FURA, R= (emission at 510 nm when excited at 340 nm - background at 510/340) / (emission at 510 nm when excited at 380 nm - background at 510/380). For FRET sensors, with excitation at 430 nm, R= (emission at 530 nm - background at 530) / (emission at 480 nm - background at 480). The FRET or FURA ratio curves were then converted to R/R_0 by dividing every R value by the average of R_2-R_8 for each trace and, when necessary, fit to a polynomial or exponential decay function to remove effects of progressive photo-bleaching or baseline drift.

REFERENCES

1. Bentley, M., Nycz, D. C., Joglekar, A., Fertschai, I., Malli, R., Graier, W. F., and Hay, J. C. (2010) Vesicular calcium regulates coat retention, fusogenicity, and size of pre-Golgi intermediates. *Mol Biol Cell*. **21**, 1033–1046
2. Helm, J. R., Bentley, M., Thorsen, K. D., Wang, T., Foltz, L., Oorschot, V., Klumperman, J., and Hay, J. C. (2014) Apoptosis-linked gene-2 (ALG-2)/Sec31 interactions regulate endoplasmic reticulum (ER)-to-Golgi transport: a potential effector pathway for luminal calcium. *J Biol Chem*. **289**, 23609–23628
3. Maki, M., Kitaura, Y., Satoh, H., Ohkouchi, S., and Shibata, H. (2002) Structures, functions and molecular evolution of the penta-EF-hand Ca2+-binding proteins. *Biochim Biophys Acta*. **1600**, 51–60
4. Yamasaki, A., Tani, K., Yamamoto, A., Kitamura, N., and Komada, M. (2006) The Ca2+-binding protein ALG-2 is recruited to endoplasmic reticulum exit sites by Sec31A and stabilizes the localization of Sec31A. *Mol Biol Cell*. **17**, 4876–4887
5. Shibata, H., Suzuki, H., Yoshida, H., and Maki, M. (2007) ALG-2 directly binds Sec31A and localizes at endoplasmic reticulum exit sites in a Ca2+-dependent manner. *Biochem Biophys Res Commun*. **353**, 756–763
6. la Cour, J. M., Mollerup, J., and Berchtold, M. W. (2007) ALG-2 oscillates in subcellular localization, unitemporally with calcium oscillations. *Biochem Biophys Res Commun*. **353**, 1063–1067
7. Shibata, H., Inuzuka, T., Yoshida, H., Sugiura, H., Wada, I., and Maki, M. (2010) The ALG-2 binding site in Sec31A influences the retention kinetics of Sec31A at the endoplasmic reticulum exit sites as revealed by live-cell time-lapse imaging. *Biosci. Biotechnol. Biochem.* **74**, 1819–1826
8. Sargeant, J., Costain, T., Madreiter-Sokolowski, C. T., Gordon, D. E., Peden, A. A., Malli, R., Graier, W. F., and Hay, J. C. (2020) Calcium Sensors ALG-2 And Peflin Bind ER Exit Sites In Alternate States To Modulate Secretion In Response To Calcium Signaling. *bioRxiv*. 10.1101/2020.02.22.944264
9. Kitaura, Y., Matsumoto, S., Satoh, H., Hitomi, K., and Maki, M. (2001) Peflin and ALG-2, members of the penta-EF-hand protein family, form a heterodimer that dissociates in a Ca2+-dependent manner. *J Biol Chem*. **276**, 14053–14058
10. Kitaura, Y., Satoh, H., Takahashi, H., Shibata, H., and Maki, M. (2002) Both ALG-2 and peflin, penta-EF-hand (PEF) proteins, are stabilized by dimerization through their fifth EF-hand regions. *Arch Biochem Biophys*. **399**, 12–18
11. Rayl, M., Truitt, M., Held, A., Sargeant, J., Thorsen, K., and Hay, J. C. (2016) Penta-EF-Hand Protein Peflin Is a Negative Regulator of ER-To-Golgi Transport. *PLoS ONE*. **11**, e0157227
12. Zhang, S., Fritz, N., Ibarra, C., and Uhlén, P. (2011) Inositol 1,4,5-trisphosphate receptor subtype-specific regulation of calcium oscillations. *Neurochem. Res.* **36**, 1175–1185
13. Nelson, O., Supnet, C., Tolia, A., Horré, K., De Strooper, B., and Bezprozvanny, I. (2011) Mutagenesis mapping of the presenilin 1 calcium leak conductance pore. *J Biol Chem*. **286**, 22339–22347
14. Klec, C., Madreiter-Sokolowski, C. T., Ziomek, G., Stryeck, S., Sachdev, V., Duta-Mare, M., Gottschalk, B., Depaoli, M. R., Rost, R., Hay, J., Waldeck-Weiermair, M., Kratky, D., Madl, T., Malli, R., and Graier, W. F. (2019) Presenilin-1 Established ER-Ca2+ Leak: a

Follow Up on Its Importance for the Initial Insulin Secretion in Pancreatic Islets and β-Cells upon Elevated Glucose. *Cell. Physiol. Biochem.* **53**, 573–586

15. Hammadi, M., Oulidi, A., Gackière, F., Katsogiannou, M., Slomianny, C., Roudbaraki, M., Dewailly, E., Delcourt, P., Lepage, G., Lotteau, S., Ducreux, S., Prevarskaya, N., and Van Coppenolle, F. (2013) Modulation of ER stress and apoptosis by endoplasmic reticulum calcium leak via translocon during unfolded protein response: involvement of GRP78. *FASEB J.* **27**, 1600–1609
16. Van Coppenolle, F., Vanden Abeele, F., Slomianny, C., Flourakis, M., Hesketh, J., Dewailly, E., and Prevarskaya, N. (2004) Ribosome-translocon complex mediates calcium leakage from endoplasmic reticulum stores. *J Cell Sci.* **117**, 4135–4142
17. Cantero-Recasens, G., Butnaru, C. M., Valverde, M. A., Naranjo, J. R., Brouwers, N., and Malhotra, V. (2018) KChIP3 coupled to Ca2+ oscillations exerts a tonic brake on baseline mucin release in the colon. *Elife*. **7**, 553
18. Stutzmann, G. E., and Mattson, M. P. (2011) Endoplasmic reticulum Ca(2+) handling in excitable cells in health and disease. *Pharmacol. Rev.* **63**, 700–727
19. Thayanidhi, N., Helm, J. R., Nycz, D. C., Bentley, M., Liang, Y., and Hay, J. C. (2010) Alpha-synuclein delays endoplasmic reticulum (ER)-to-Golgi transport in mammalian cells by antagonizing ER/Golgi SNAREs. *Mol Biol Cell*. **21**, 1850–1863
20. Chen, R., Valencia, I., Zhong, F., McColl, K. S., Roderick, H. L., Bootman, M. D., Berridge, M. J., Conway, S. J., Holmes, A. B., Mignery, G. A., Velez, P., and Distelhorst, C. W. (2004) Bcl-2 functionally interacts with inositol 1,4,5-trisphosphate receptors to regulate calcium release from the ER in response to inositol 1,4,5-trisphosphate. *J. Cell Biol.* **166**, 193–203
21. Hay, J. C., Klumperman, J., Oorschot, V., Steegmaier, M., Kuo, C. S., and Scheller, R. H. (1998) Localization, dynamics, and protein interactions reveal distinct roles for ER and Golgi SNAREs. *J. Cell Biol.* **141**, 1489–1502
22. Thillaiappan, N. B., Chakraborty, P., Hasan, G., and Taylor, C. W. (2019) IP3 receptors and Ca2+ entry. *Biochim Biophys Acta Mol Cell Res*. **1866**, 1092–1100
23. Hattori, M., Suzuki, A. Z., Higo, T., Miyauchi, H., Michikawa, T., Nakamura, T., Inoue, T., and Mikoshiba, K. (2004) Distinct roles of inositol 1,4,5-trisphosphate receptor types 1 and 3 in Ca2+ signaling. *J Biol Chem*. **279**, 11967–11975
24. Almirza, W. H. M., Peters, P. H. J., van Meerwijk, W. P. M., van Zoelen, E. J. J., and Theuvenet, A. P. R. (2010) Different roles of inositol 1,4,5-trisphosphate receptor subtypes in prostaglandin F(2alpha)-induced calcium oscillations and pacemaking activity of NRK fibroblasts. *Cell Calcium*. **47**, 544–553
25. Leybaert, L., and Sanderson, M. J. (2012) Intercellular Ca(2+) waves: mechanisms and function. *Physiol. Rev.* **92**, 1359–1392
26. Palmer, A. E., Jin, C., Reed, J. C., and Tsien, R. Y. (2004) Bcl-2-mediated alterations in endoplasmic reticulum Ca2+ analyzed with an improved genetically encoded fluorescent sensor. *Proc Natl Acad Sci USA*. **101**, 17404–17409
27. Palmer, A. E., Giacomello, M., Kortemme, T., Hires, S. A., Lev-Ram, V., Baker, D., and Tsien, R. Y. (2006) Ca2+ indicators based on computationally redesigned calmodulin-peptide pairs. *Chem. Biol.* **13**, 521–530
28. Palmer, A. E., and Tsien, R. Y. (2006) Measuring calcium signaling using genetically targetable fluorescent indicators. *Nat Protoc*. **1**, 1057–1065

29. Eckenrode, E. F., Yang, J., Velmurugan, G. V., Foskett, J. K., and White, C. (2010) Apoptosis protection by Mcl-1 and Bcl-2 modulation of inositol 1,4,5-trisphosphate receptor-dependent Ca2+ signaling. *J Biol Chem*. **285**, 13678–13684
30. Müller, M., Cheung, K.-H., and Foskett, J. K. (2011) Enhanced ROS generation mediated by Alzheimer's disease presenilin regulation of InsP3R Ca2+ signaling. *Antioxid Redox Signal*. **14**, 1225–1235
31. Takada, S. H., Ikebara, J. M., de Sousa, E., Cardoso, D. S., Resende, R. R., Ulrich, H., Rückl, M., Rüdiger, S., and Kihara, A. H. (2017) Determining the Roles of Inositol Trisphosphate Receptors in Neurodegeneration: Interdisciplinary Perspectives on a Complex Topic. *Mol Neurobiol*. **54**, 6870–6884
32. Ananthanarayanan, M., Banales, J. M., Guerra, M. T., Spirli, C., Munoz-Garrido, P., Mitchell-Richards, K., Tafur, D., Saez, E., and Nathanson, M. H. (2015) Post-translational regulation of the type III inositol 1,4,5-trisphosphate receptor by miRNA-506. *J Biol Chem*. **290**, 184–196
33. Kuchay, S., Giorgi, C., Simoneschi, D., Pagan, J., Missiroli, S., Saraf, A., Florens, L., Washburn, M. P., Collazo-Lorduy, A., Castillo-Martin, M., Cordon-Cardo, C., Sebti, S. M., Pinton, P., and Pagano, M. (2017) PTEN counteracts FBXL2 to promote IP3R3- and Ca2+-mediated apoptosis limiting tumour growth. *Nature*. **546**, 554–558
34. Bononi, A., Giorgi, C., Patergnani, S., Larson, D., Verbruggen, K., Tanji, M., Pellegrini, L., Signorato, V., Olivetto, F., Pastorino, S., Nasu, M., Napolitano, A., Gaudino, G., Morris, P., Sakamoto, G., Ferris, L. K., Danese, A., Raimondi, A., Tacchetti, C., Kuchay, S., Pass, H. I., Affar, E. B., Yang, H., Pinton, P., and Carbone, M. (2017) BAP1 regulates IP3R3-mediated Ca2+ flux to mitochondria suppressing cell transformation. *Nature*. **546**, 549–553
35. Weerachayaphorn, J., Amaya, M. J., Spirli, C., Chansela, P., Mitchell-Richards, K. A., Ananthanarayanan, M., and Nathanson, M. H. (2015) Nuclear Factor, Erythroid 2-Like 2 Regulates Expression of Type 3 Inositol 1,4,5-Trisphosphate Receptor and Calcium Signaling in Cholangiocytes. *Gastroenterology*. **149**, 211–222.e10
36. Franca, A., Carlos Melo Lima Filho, A., Guerra, M. T., Weerachayaphorn, J., Loiola Dos Santos, M., Njei, B., Robert, M., Xavier Lima, C., Vieira Teixeira Vidigal, P., Banales, J. M., Ananthanarayanam, M., Leite, M. F., and Nathanson, M. H. (2019) Effects of Endotoxin on Type 3 Inositol 1,4,5-Trisphosphate Receptor in Human Cholangiocytes. *Hepatology*. **69**, 817–830
37. Kuga, N., Sasaki, T., Takahara, Y., Matsuki, N., and Ikegaya, Y. (2011) Large-scale calcium waves traveling through astrocytic networks in vivo. *J Neurosci*. **31**, 2607–2614
38. Kurth-Nelson, Z. L., Mishra, A., and Newman, E. A. (2009) Spontaneous glial calcium waves in the retina develop over early adulthood. *J Neurosci*. **29**, 11339–11346
39. Fontana, J. M., Khodus, G. R., Unnersjö-Jess, D., Blom, H., Aperia, A., and Brismar, H. (2019) Spontaneous calcium activity in metanephric mesenchymal cells regulates branching morphogenesis in the embryonic kidney. *FASEB J*. **33**, 4089–4096
40. Weissman, T. A., Riquelme, P. A., Ivic, L., Flint, A. C., and Kriegstein, A. R. (2004) Calcium waves propagate through radial glial cells and modulate proliferation in the developing neocortex. *Neuron*. **43**, 647–661
41. Dong, Y., Lee, Y., Cui, K., He, M., Wang, B., Bhattacharjee, S., Zhu, B., Yago, T., Zhang, K., Deng, L., Ouyang, K., Wen, A., Cowan, D. B., Song, K., Yu, L., Brophy, M. L., Liu, X., Wylie-Sears, J., Wu, H., Wong, S., Cui, G., Kawashima, Y., Matsumoto, H.,

Kodera, Y., Wojcikiewicz, R. J. H., Srivastava, S., Bischoff, J., Wang, D.-Z., Ley, K., and Chen, H. (2020) Epsin-mediated degradation of IP3R1 fuels atherosclerosis. *Nat Commun*. **11**, 3984–16

42. Berridge, M. J. (2016) The Inositol Trisphosphate/Calcium Signaling Pathway in Health and Disease. *Physiol. Rev.* **96**, 1261–1296
43. Mangla, A., Guerra, M. T., and Nathanson, M. H. (2020) Type 3 inositol 1,4,5-trisphosphate receptor: A calcium channel for all seasons. *Cell Calcium*. **85**, 102132
44. Shibao, K., Fiedler, M. J., Nagata, J., Minagawa, N., Hirata, K., Nakayama, Y., Iwakiri, Y., Nathanson, M. H., and Yamaguchi, K. (2010) The type III inositol 1,4,5-trisphosphate receptor is associated with aggressiveness of colorectal carcinoma. *Cell Calcium*. **48**, 315–323
45. Mound, A., Vautrin-Glabik, A., Foulon, A., Botia, B., Hague, F., Parys, J. B., Ouadid-Ahidouch, H., and Rodat-Despoix, L. (2017) Downregulation of type 3 inositol (1,4,5)-trisphosphate receptor decreases breast cancer cell migration through an oscillatory Ca2+ signal. *Oncotarget*. **8**, 72324–72341
46. Szatkowski, C., Parys, J. B., Ouadid-Ahidouch, H., and Matifat, F. (2010) Inositol 1,4,5-trisphosphate-induced Ca2+ signalling is involved in estradiol-induced breast cancer epithelial cell growth. *Mol Cancer*. **9**, 156–13
47. Hamamori, Y., Hoshijima, M., Ohmori, T., Ueda, T., and Takai, Y. (1988) Serotonin as a major serum factor inducing the phospholipase C-mediated hydrolysis of phosphoinositides in normal rat kidney cells. *Cancer Res*. **48**, 6697–6702
48. Maki, M., and Shibata, H. (2007) The penta-EF-hand protein ALG-2 and its interacting proteins. *Calcium Binding Proteins*
49. Lodish, H. F., and Kong, N. (1990) Perturbation of cellular calcium blocks exit of secretory proteins from the rough endoplasmic reticulum. *J Biol Chem*. **265**, 10893–10899
50. Chen, J.-L., Ahluwalia, J. P., and Stamnes, M. (2002) Selective effects of calcium chelators on anterograde and retrograde protein transport in the cell. *J Biol Chem*. **277**, 35682–35687
51. Chakraborty, S., Deb, B. K., Chorna, T., Konieczny, V., Taylor, C. W., and Hasan, G. (2016) Mutant IP3 receptors attenuate store-operated Ca2+ entry by destabilizing STIM-Orai interactions in Drosophila neurons. *J Cell Sci*. **129**, 3903–3910
52. Xu, D., and Hay, J. C. (2004) Reconstitution of COPII vesicle fusion to generate a pre-Golgi intermediate compartment. **167**, 997–1003
53. Wang, T., Grabski, R., Sztul, E., and Hay, J. C. (2015) p115-SNARE interactions: a dynamic cycle of p115 binding monomeric SNARE motifs and releasing assembled bundles. *Traffic*. **16**, 148–171

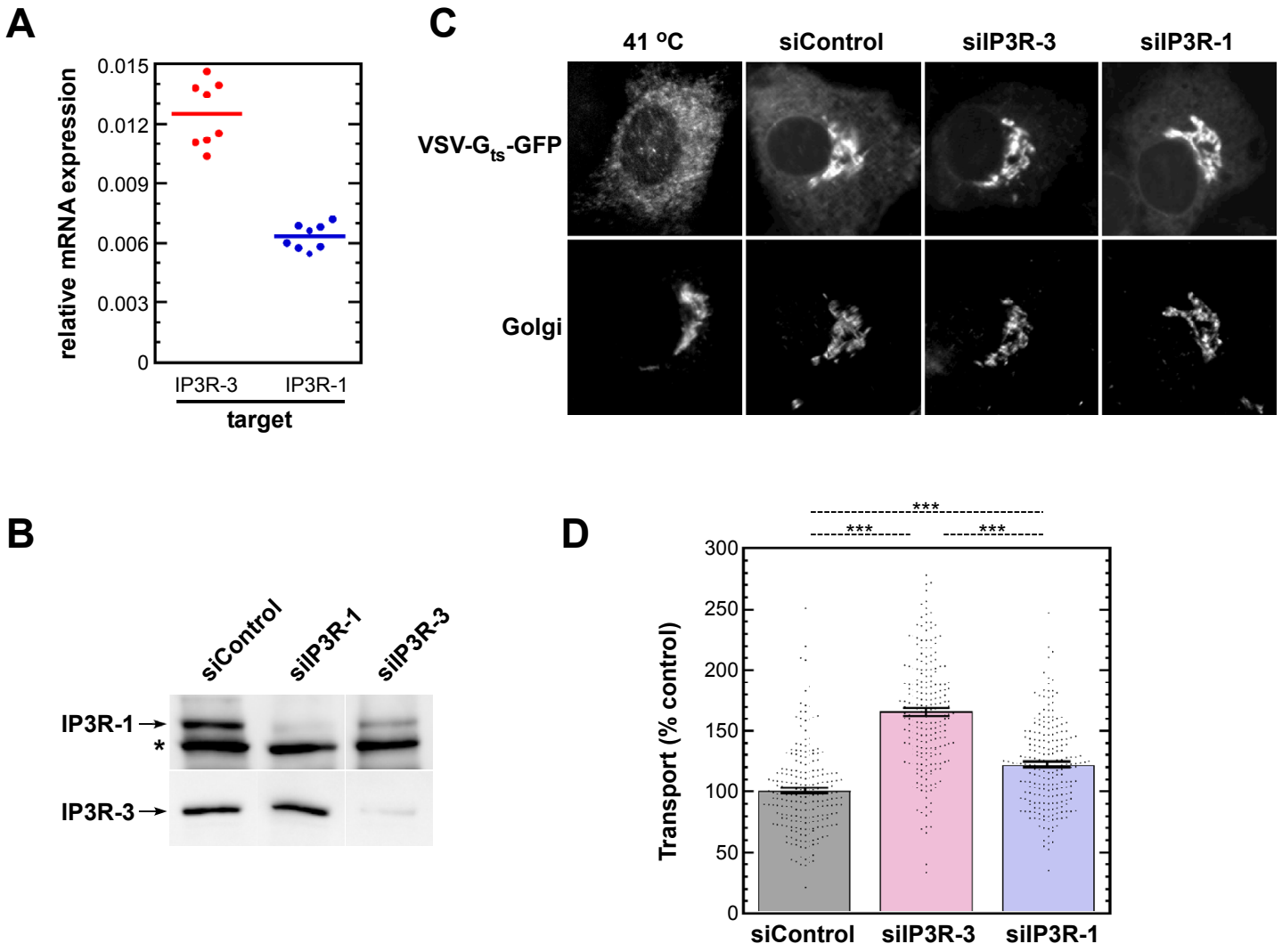

Figure 1. Expression of IP3 receptors regulates ER-to-Golgi transport in NRK cells. (A) Expression ratio of IP3R-1 and IP3R-3 in NRK cells analyzed by qRT-PCR. The quantity of each target RNA is normalized to that determined for GAPDH in parallel reactions. **(B)** Verification by immunoblot of IP3R depletions using isoform-specific siRNAs. Asterisk marks an unknown nonspecific band recognized by the anti-IP3R-1 antibody. **(C)** Representative images of NRK cells from the ER-to-Golgi transport assay quantified in D. NRK cells were transfected with VSV-G_{ts045}-GFP with or without siRNAs as indicated. Following growth at 41 ºC for 48 h, cells were shifted to 32 ºC for 10 min, to permit transport, prior to fixation. Fixed cells were immuno-labeled with mannosidase II and imaged by widefield microscopy; VSV-G-GFP and mannosidase II channels are displayed for each cell. **(D)** Each transfected cell was assigned a transport index representing trafficking of VSV-G based upon the ratio of Golgi to peripheral green fluorescence. The transport index of each individual cell is plotted. 200-300 cells were randomly quantified from each condition, and results shown are representative of at least three experiments with consistent trends. p-values for two-tailed Student T-tests with unequal variance are indicated above; * = $p \leq .05$; ** = $p \leq .005$; *** = $p \leq .0005$. Standard error is shown for each plot.

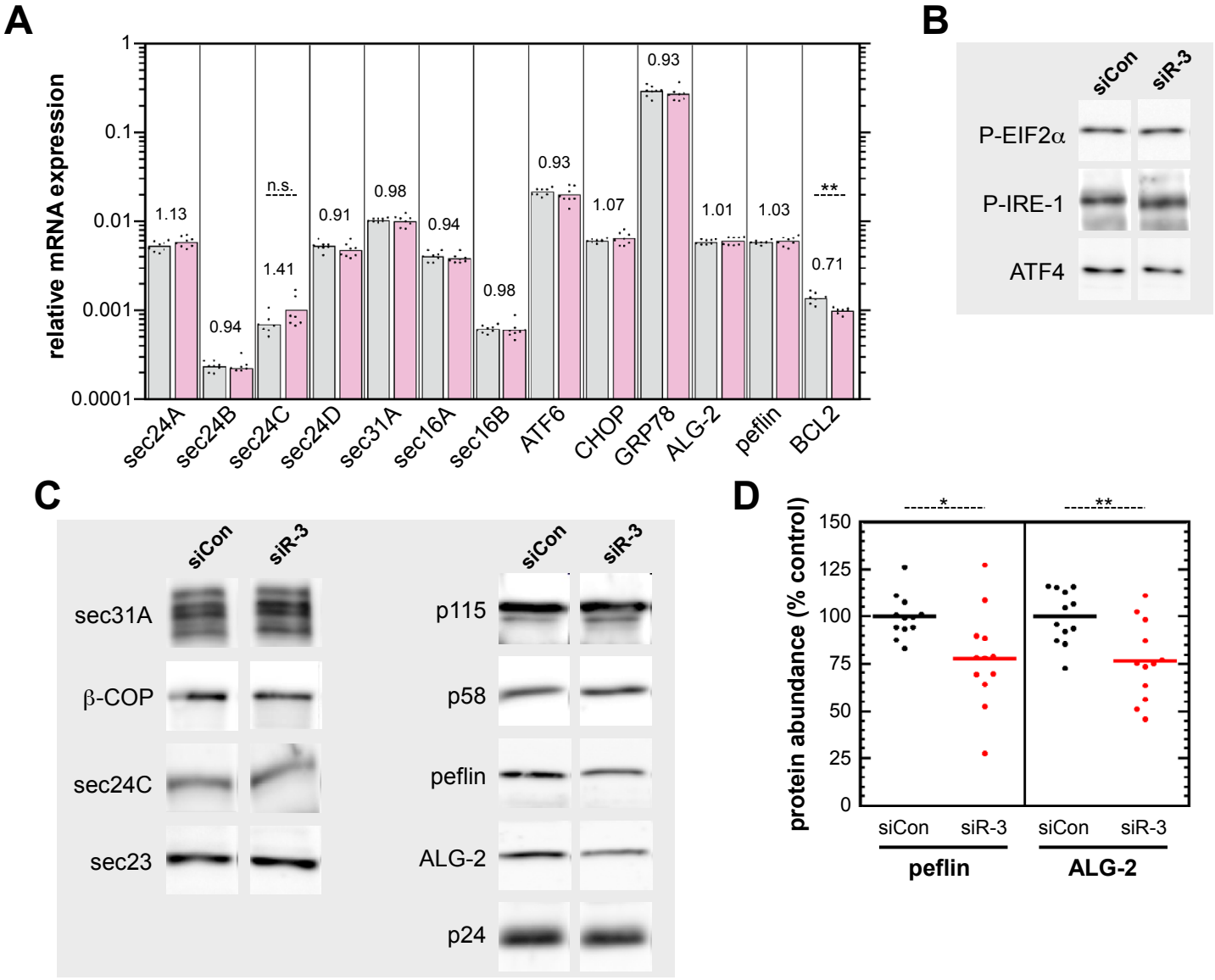

Figure 2. IP3R depletion destabilizes ALG-2 and peflin but does not affect expression of other ER export machinery. (A) NRK cells were transfected with control (gray) or IP3R-3 (light red) siRNAs, grown for 48 h, lysed and then mRNA was analyzed by qRT-PCR to detect expression of trafficking and other proteins. The quantity of each target RNA is normalized to that determined for GAPDH in parallel reactions. Value labels indicate the ratio of expression in siR-3 cells to that of control cells. **(B, C)** Immunoblots of ER stress proteins (B) and ER/Golgi trafficking machinery (C) in NRK cell extracts, 48 h after transfection with control or IP3R-3 siRNAs. No significant changes were observed, except for decreases in ALG-2 and peflin. **(D)** Quantitation of multiple technical replicates from several different experiments documented effects of IP3R-3 depletion on ALG-2 and peflin protein abundance.

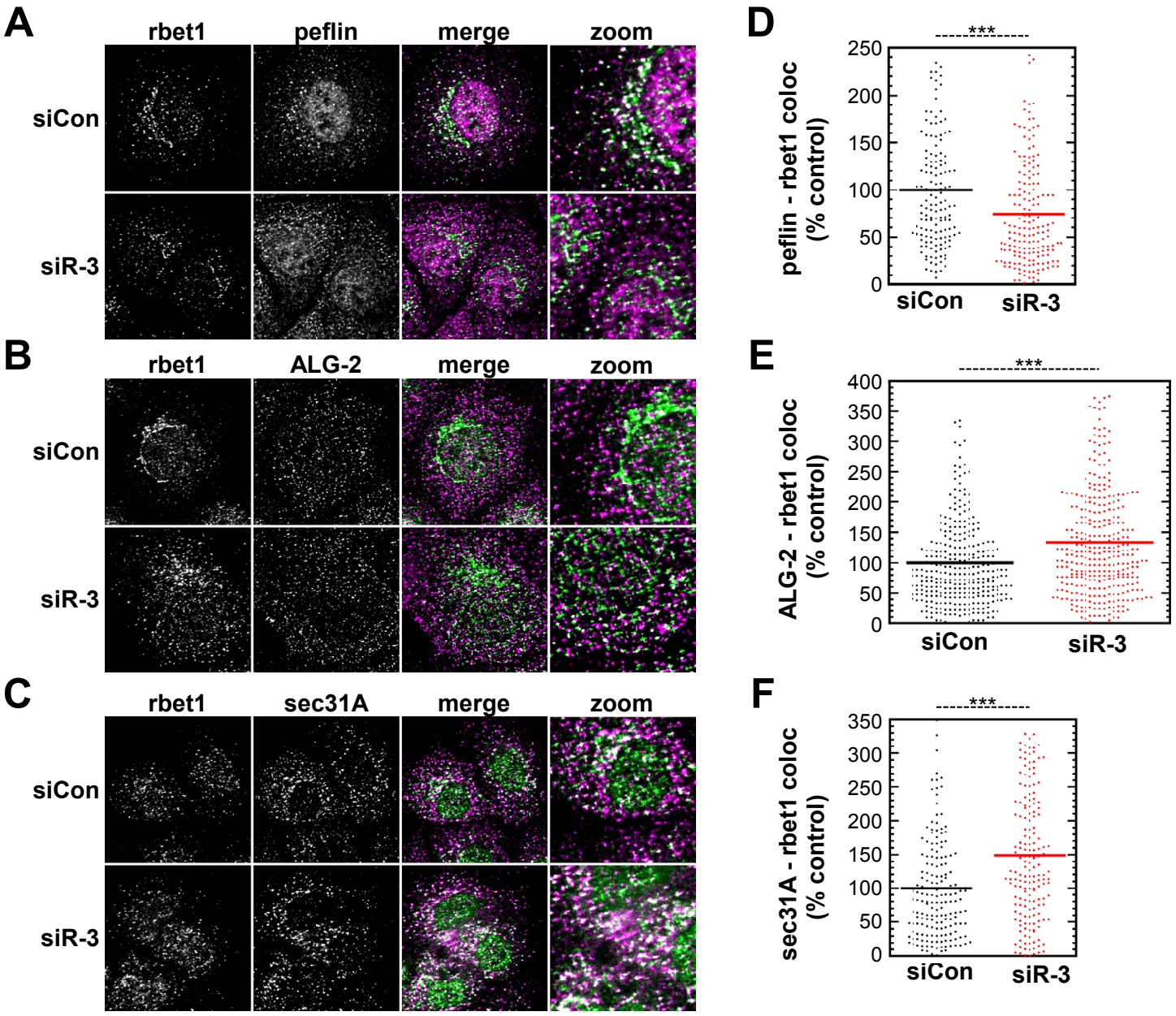

Figure 3. IP3R depletion causes a decrease in peflin and increases in ALG-2 and sec31A at ERES. (A-C) NRK cells were transfected with the indicated siRNAs. After 48 h, cells were fixed and immunolabeled for endogenous rbet1, peflin, ALG-2, or sec31A, as indicated. Representative micrographs are shown. **(D-F)** Object analysis on ~150 cells (D, F) or ≥300 cells (E) per condition to quantify overlap between rbet1 objects and the other labeled proteins.

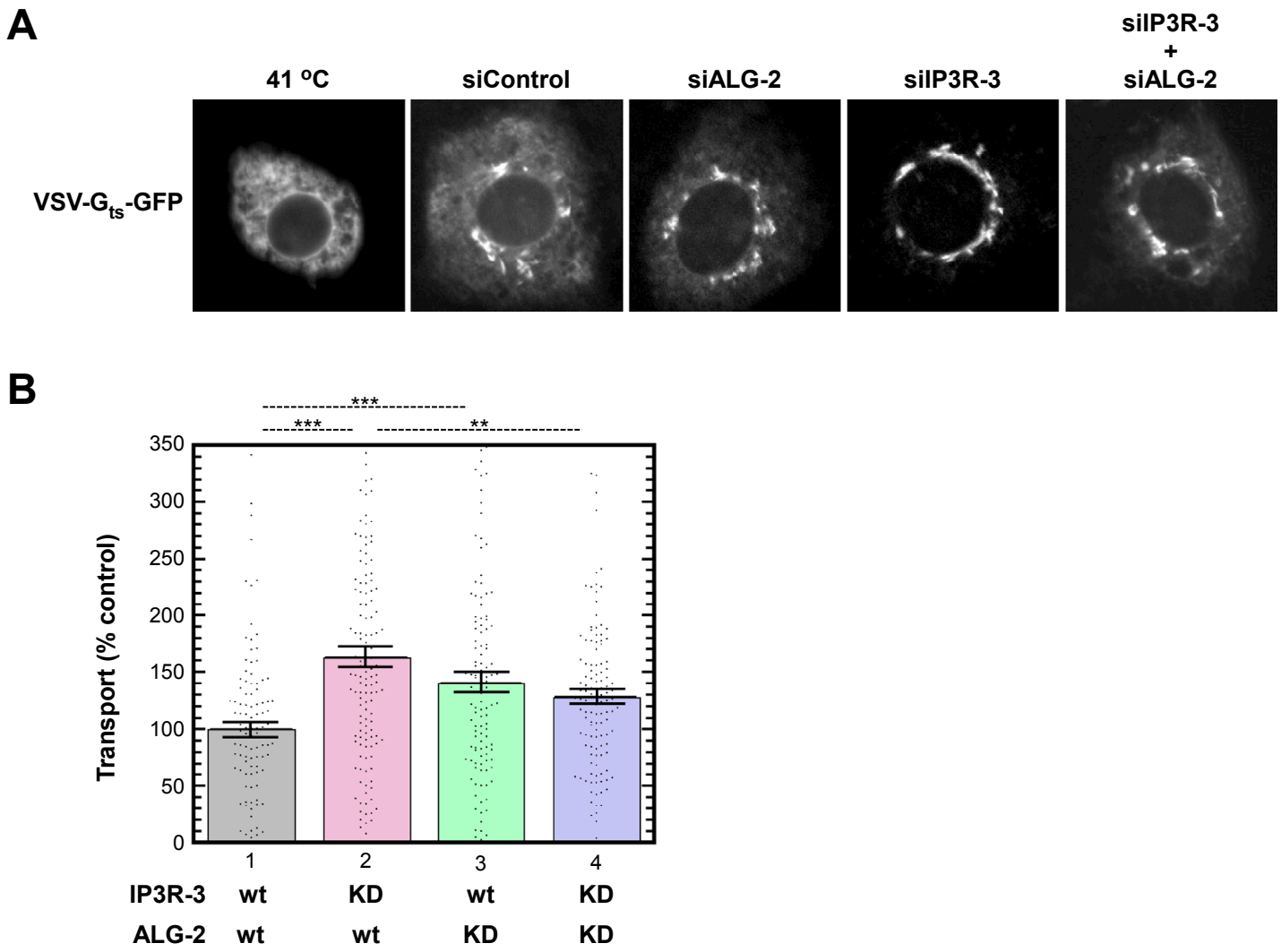

Figure 4. IP3R regulation of ER export requires ALG-2. In the absence of ALG-2, IP3R depletion fails to increase secretion. **(A)** Representative images of NRK cells from the ER-to-Golgi transport assay quantified in B (see Figure 1 legend for more detail); VSV-G-GFP is displayed for each representative cell. **(B)** Quantification of ≥100 cells for each condition from A (see Figure 1 legend for more detail).

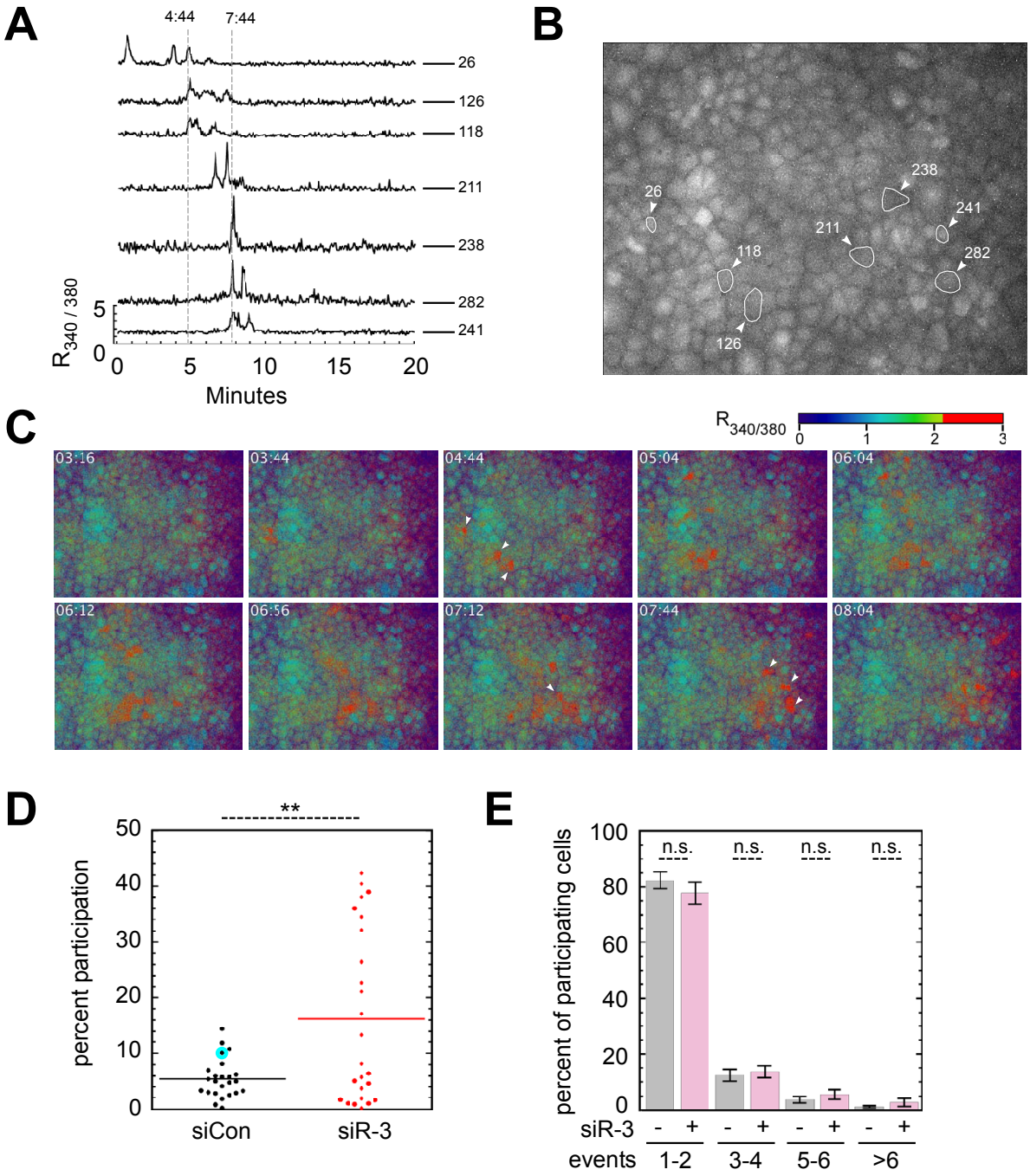

Figure 5. IP3R depletion caused increased spontaneous Ca^{2+} oscillations. (A) Individual FURA-2 cytosolic Ca^{2+} traces of 7 control NRK cells in one field. **(B)** Group of 338 cells containing the same cells plotted in A, with their individual locations marked. **(C)** $R_{340/380}$ heatmap of field in B at distinct timepoints. White arrows indicate position and time of major cytosolic Ca^{2+} signals in cells from A. **(D)** Quantitation of cells participating in spontaneous cytosolic Ca^{2+} signals during the 20-minute imaging period as in A, with each dot summarizing a run of ~500 cells. The particular run shown in A-C is highlighted in cyan. **(E)** Quantitation of number of oscillations per cell from D, as percent of all cells with oscillations.

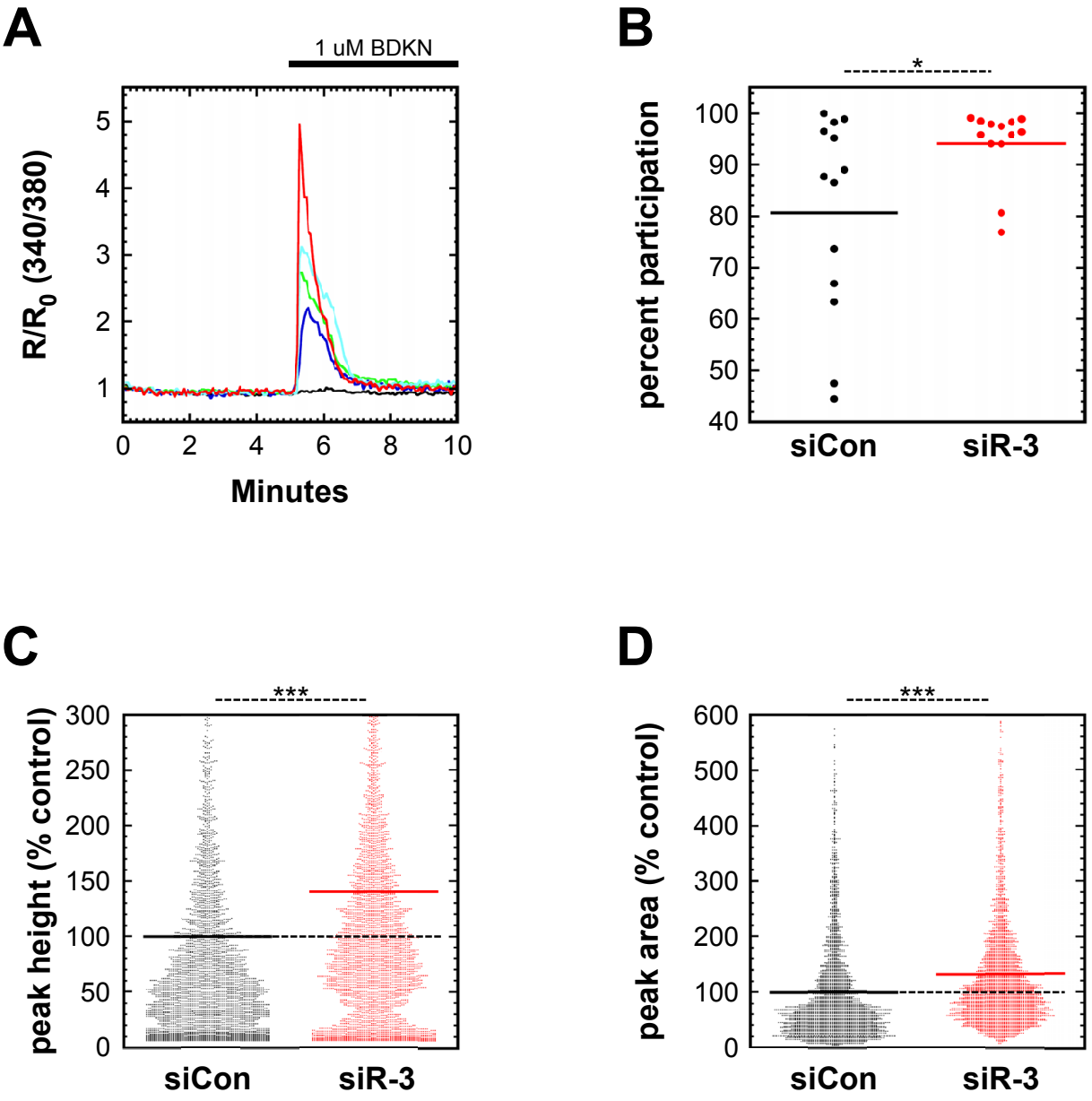

Figure 6. IP3R depletion potentiates agonist-dependent Ca^{2+} signaling. (A) FURA-2 cytosolic Ca^{2+} recording of 5 control NRK cells in one field upon stimulation with 1 μM extracellular bradykinin (BDKN). Four cells displayed cytosolic Ca^{2+} signals of varying sizes while one (black trace) remained inactive. **(B)** Quantitation of the percentage of cells in one field responding to BDKN stimulation as in A. Each field contained a total of ~300 cells. **(C,D)** Quantitation of peak height (defined as change from average baseline value) (C) and peak area (D) from traces of BDKN-responsive cells. Results in B-D consist of three replicate experiments combined. Cells were defined as BDKN-responsive in B if their peak height was ≥0.1. In C and D, each dot represents one cell (N≈4000 cells per condition).

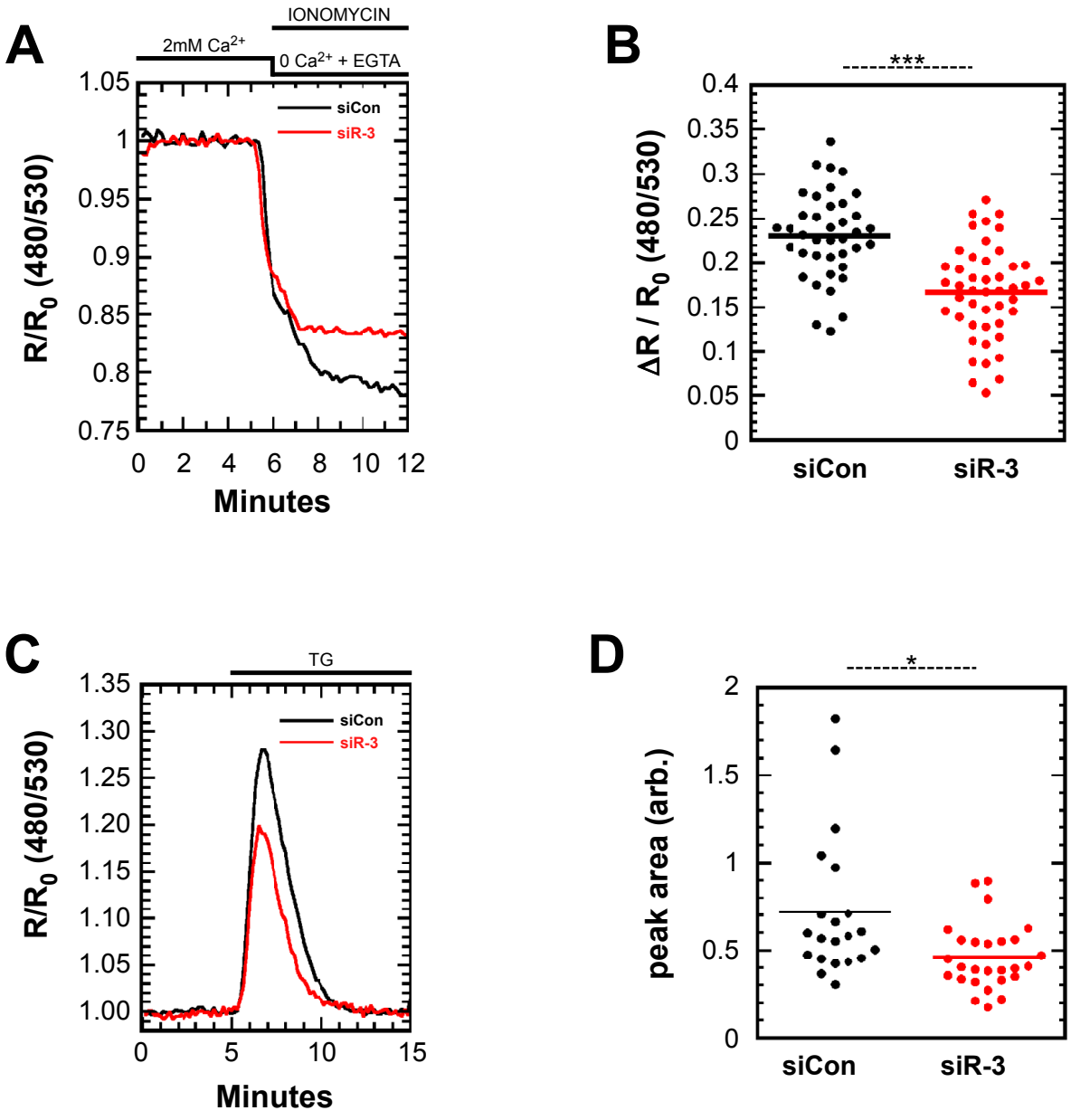

Figure 7. IP3R depletion causes reduced ER luminal Ca^{2+} stores. (A) Representative traces of ER luminal Ca^{2+}, using the sensor D1ER, upon depletion with ionomycin and low Ca^{2+} medium. **(B)** Quantitation of the luminal Ca^{2+} drops in many cells from three experiments of Ca^{2+} depletion traces as in A. **(C)** Representative traces of cytosolic Ca^{2+}, using the sensor D3cpv, upon release of luminal Ca^{2+} stores by addition of thapsigargin to the extracellular medium. **(D)** Quantitation of multiple cells from two experiments of the peak areas in traces as in C. In B and D, each dot represents one cell.

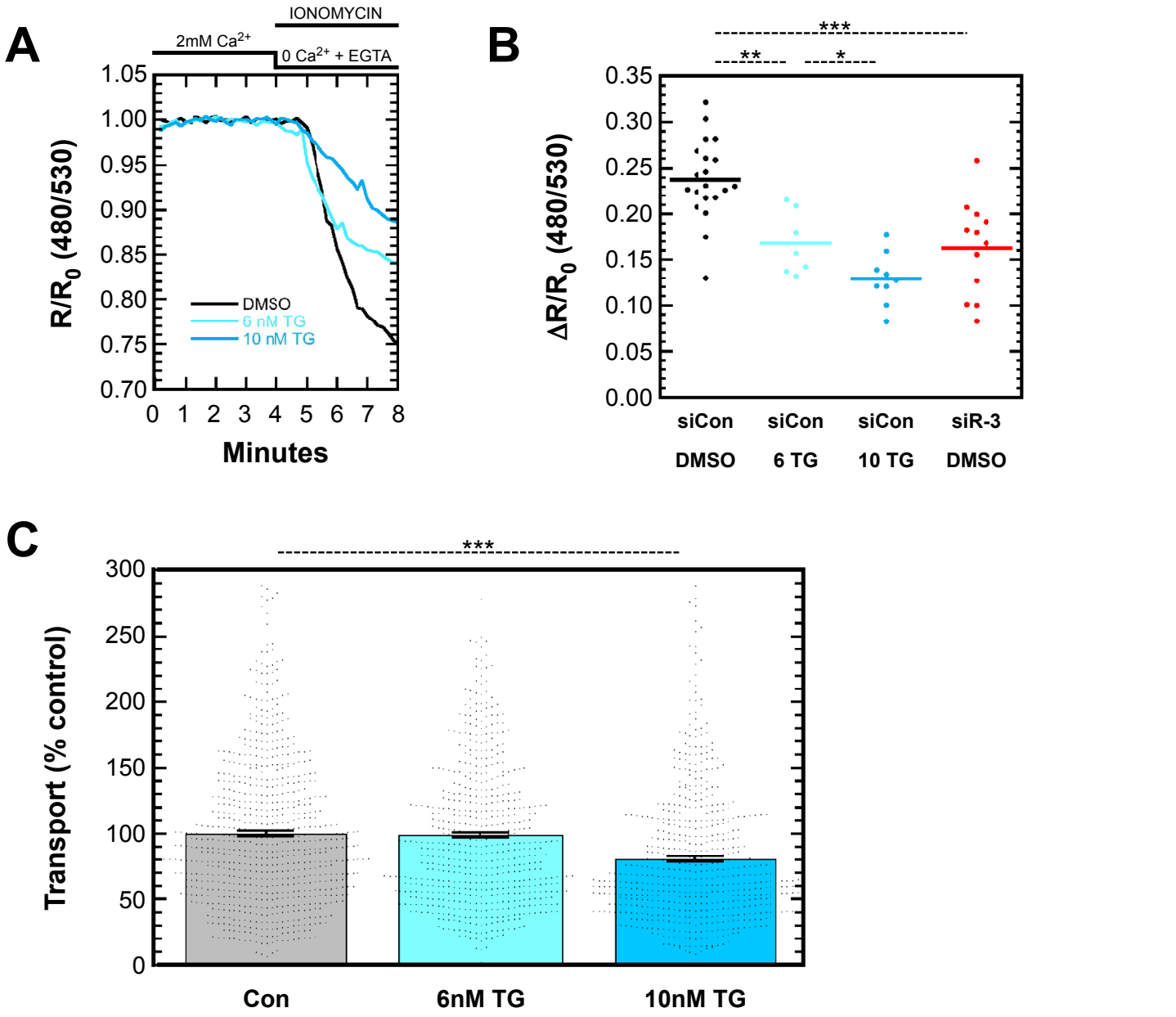

Figure 8. Partial depletion of luminal Ca^{2+} stores in the absence of IP3R siRNA does not increase ER export. (A) D1ER-transfected NRK cells were pretreated for 24 h with DMSO, 6 or 10 nM Tg, as indicated, and then depleted of ER luminal Ca^{2+} with ionomycin and low Ca^{2+} medium as in Figure 7. Shown are representative traces of the ER luminal Ca^{2+}drop as reported by D1ER. **(B)** 6 nM Tg lowers ER Ca^{2+} stores similarly to that of IP3R-3 siRNA. Cells were transfected with D1ER and an siRNA, and pretreated for 24 h with DMSO, 6 or 10 nM Tg, as indicated, and then depleted of ER luminal Ca^{2+} as in A. The luminal Ca^{2+} drops from individual cells in two experiments were quantitated and combined. **(C)** 6 nM Tg does not affect ER-to-Golgi transport rates, whereas 10 nM inhibits by 20%. NRK cells were transfected with VSV_{ts045}-G-GFP and pretreated with DMSO, 6 or 10 nM Tg, as indicated, and then ER-to-Golgi transport was measured as in Figures 1 and 4. Results from ≥600 cells per condition from several experiments are combined.